DOI: 10.1002/chem.201000210

Luminescent Amphiphilic 2,6-Bis(1-alkylpyrazol-3-yl)pyridyl Platinum(II) Complexes: Synthesis, Characterization, Electrochemical, Photophysical, and Langmuir–Blodgett Film Formation Studies

Le Zhao,[a] Keith Man-Chung Wong,*[b] Bao Li,[a] Wen Li,[a] Nianyong Zhu,[b] Lixin Wu,*[a] and Vivian Wing-Wah Yam*[a, b]

Abstract: Two series of novel platinum(II) 2,6-bis(1-alkylpyrazol-3-yl)pyridyl (N5C*n*) complexes, [Pt(N5C*n*)Cl][X] (**1**–**9**) and [Pt(N5C*n*)(C≡CR)][X] (**10**–**13**) (X = trifluoromethanesulfonate (OTf) or PF_6; R = C_6H_5, C_6H_4-*p*-CF_3 and C_6H_4-*p*-N(C_6H_5)$_2$), with various chain lengths of the alkyl groups on the nitrogen atom of the pyrazolyl units have been successfully synthesized and characterized. Their electrochemical and photophysical properties have been studied. Some of their molecular structures have also been determined by X-ray crystallography. Two amphiphilic platinum(II) 2,6-bis(1-tetradecylpyrazol-3-yl)pyridyl (N5C14) complexes, [Pt(N5C14)Cl]PF_6 (**7**) and [Pt(N5C14)(C≡CC_6H_5)]PF_6 (**13**), were found to form stable and reproducible Langmuir–Blodgett (LB) films at the air–water interface. The characterization of such LB films has been investigated by the study of their surface pressure–area (π–A) isotherms, UV/Vis spectroscopy, XRD, X-ray photoelectron spectroscopy (XPS), FTIR, and polarized IR spectroscopy. The luminescence property of **13** in LB films has also been studied.

Keywords: amphiphiles · Langmuir–Blodgett films · luminescence · platinum · X-ray diffraction

Introduction

The spectroscopic and photophysical behavior of square-planar platinum(II) complexes has been extensively studied in the past few decades, due to their intriguing spectroscopic and photophysical properties associated with the occurrence of Pt···Pt and π–π interactions.[1–7] Examples include the Magnus' salt of $[Pt(NH_3)_4][PtCl_4]$,[1a] $[Pt_2(pop)_4]^{4-}$ (pop = $P_2O_5H_2^{2-}$ diphosphonate),[1b] and various double salts, such as $[Pt(CNR)_4][Pt(CN)_4]$,[1c–e] which exhibit rich luminescence, photochemistry, vapochromic, and vapoluminescence behavior. Another class of such compounds is the platinum(II) polypyridyl complexes that show rich polymorphism in the solid state. Such polymorphic phenomena and the variation of luminescence colors, dependent upon the temperature, type of counterion, and solvents used for crystallization, are attributed to the extent of metal···metal interactions and π–π stacking of the polypyridyl ligands.[2–6,8] Apart from the photophysical studies, platinum(II) complexes with square-planar geometry have also attracted considerable attention as a result of their interesting biological activities,[9] such as antitumor cytotoxicity, DNA intercalation, and protein binding behavior.

Our group has reported the first preparation of luminescent alkynylplatinum(II) terpyridyl complexes.[5a] Compared with the chloroplatinum(II) analogues, which are nonemissive in the fluid solution at room temperature, the luminescence properties of the alkynylplatinum(II) terpyridyl system have been enhanced upon replacement of the chloro ligand with an alkynyl group. It was suggested that the nonradiative deactivation through the d–d ligand-field (LF) state is reduced as a result of a larger d–d LF splitting by the effect of the coordination of the strongly σ-donating alkynyl ligand. The luminescence origins are from the triplet

[a] L. Zhao, Dr. B. Li, Dr. W. Li, Prof. Dr. L. Wu, Prof. Dr. V. W.-W. Yam
State Key Laboratory of Supramolecular Structure and Materials
Jilin University, Changchun (P.R. China)
Fax: (+86) 431-8519-3421
E-mail: wulx@jlu.edu.cn

[b] Dr. K. M.-C. Wong, Dr. N. Zhu, Prof. Dr. V. W.-W. Yam
Institute of Molecular Functional Materials and
Department of Chemistry, The University of Hong Kong
Pokfulam Road, Hong Kong (P.R. China)
Fax: (+852) 2857-1586
E-mail: wongmc@hku.hk
wwyam@hku.hk

Supporting information for this article is available on the WWW under http://dx.doi.org/10.1002/chem.201000210.

excited state of (dπ(Pt)→π*(trpy)) (trpy = terpyridyl) metal-to-ligand charge transfer (MLCT) mixed with (pπ(C≡C)→π*(trpy)) ligand-to-ligand charge transfer (LLCT) character. The spectroscopic behavior would be perturbed by modification of the lowest-energy excited states and, as a consequence, the emission color could be fine-tuned. In the presence of the various stimuli, including pH and metal cations, their electronic absorption and luminescence spectra were found to show changes to give the respective colorimetric and luminescence sensors.[5a,8] Studies on the related alkynylplatinum(II) terpyridyl system also showed that drastic changes in the solution color and luminescence enhancement could be brought about by solvent-induced aggregation in mixed solvent systems through metal···metal and π–π interactions.[5b,c] Similar spectroscopic changes have also been observed due to aggregate formation induced by the electrostatic assembly in the presence of anionic polyelectrolytes.[6a,b,g] Extension of the work to dinuclear complexes with a flexible bridge[6d] and metallogel formation,[6e,f] involving interesting color changes through intramolecular and intermolecular aggregation or deaggregation processes, has also been made.

Another square-planar chloroplatinum(II) complex of [Pt(bzimpy)Cl]$^+$, with 2,6-bis(*N*-alkylbenzimidazol-2′-yl)pyridine as the tridentate ligand, has been explored by Haga and co-workers.[10a] The amphiphilic platinum(II) complex containing 2,6-bis(1-octadecylbenzimidazol-2-yl)pyridine was found to form stable and reproducible Langmuir–Blodgett (LB) multilayer films. Strong emission from both the multilayer LB films, as well as the monolayer was observed. The aggregation[10a–c] and fluorescence resonance energy transfer (FRET)[10d] properties have also been investigated. By employing a similar synthetic methodology and approach as that for alkynylplatinum(II) terpyridyl complexes, a related class of luminescent alkynylplatinum(II) 2,6-bis(*N*-alkylbenzimidazol-2′-yl)pyridyl complexes has been reported and shown to display interesting dual luminescence behavior, depending on the polarity of the solvents, and gelation properties.[7] Some of them demonstrated a unique example of metallogels that show an unusual luminescence enhancement during the gel-to-sol phase transition upon increasing the temperature.[7b]

Similar to the 2,6-bis(*N*-alkylbenzimidazol-2′-yl)pyridine, which serves as a terpyridine substitute to construct transition metal complexes of ruthenium(II),[11] copper(I),[12] iron(II),[13a] and iridium(III),[13d] derivatives of 2,6-di(pyrazol-1-yl)pyridine and 2,6-di(pyrazol-3-yl)pyridine have also been employed as another class of tridentate N-donor ligands for transition-metal and lanthanide ions in the past two decades.[14] The advantages and disadvantages of such tridentate ligands, relative to the widely investigated terpyridine, have been described in a recent review.[14a] Chloroplatinum(II) and phenylplatinum(II) complexes of 2,6-di(pyrazol-1-yl)pyridine and 2,6-di(3,5-dimethylpyrazol-1-yl)pyridine have been prepared by Connick and co-workers.[14b] Electrochemical and UV/Vis absorption studies showed that 2,6-di(pyrazol-1-yl)pyridine is a weaker σ-donor and π-acceptor than terpyridine, and one of the complexes was found to exhibit a remarkably intense emission in the solid state at 77 K.

Despite their superficial similarity, it is anticipated that the chemistry of 2,6-di(pyrazol-1-yl)pyridines and 2,6-di(pyrazol-3-yl)pyridines is not the same. However, the related platinum(II) complexes of 2,6-di(pyrazol-3-yl)pyridine are not known. Herein, we report the synthesis and isolation of a new class of platinum(II) 2,6-bis(1-alkylpyrazol-3-yl)pyridyl (N5C*n*) complexes, [Pt(N5C*n*)Cl][X] (**1**–**9**) and [Pt(N5C*n*)(C≡CR)][X] (**10**–**13**) (X = trifluoromethanesulfonate (OTf) or PF_6; R = C_6H_5, C_6H_4-*p*-CF_3 and C_6H_4-*p*-$N(C_6H_5)_2$), with various chain lengths of the alkyl groups on the nitrogen atom of the pyrazolyl units (Scheme 1). The X-ray crystal structures of some of them have been determined. The electrochemical and electronic absorption properties of all the complexes have been studied. The alkynylplatinum(II) complexes were found to exhibit rich photoluminescence behavior. Two amphiphilic platinum(II) 2,6-bis(1-tetradecylpyrazol-3-yl)pyridyl (N5C14) complexes, [Pt(N5C14)Cl]PF_6 (**7**) and [Pt(N5C14)(C≡CC_6H_5)]PF_6 (**13**), were found to form stable and reproducible LB films at the air–water interface. The characterization of such LB films was achieved by the study of their surface pressure–area (π–A) isotherms, UV/Vis spectroscopy, XRD, X-ray photoelectron spectroscopy (XPS), FTIR, and polarized IR spectroscopy. The luminescence properties of **13** in LB films were also investigated.

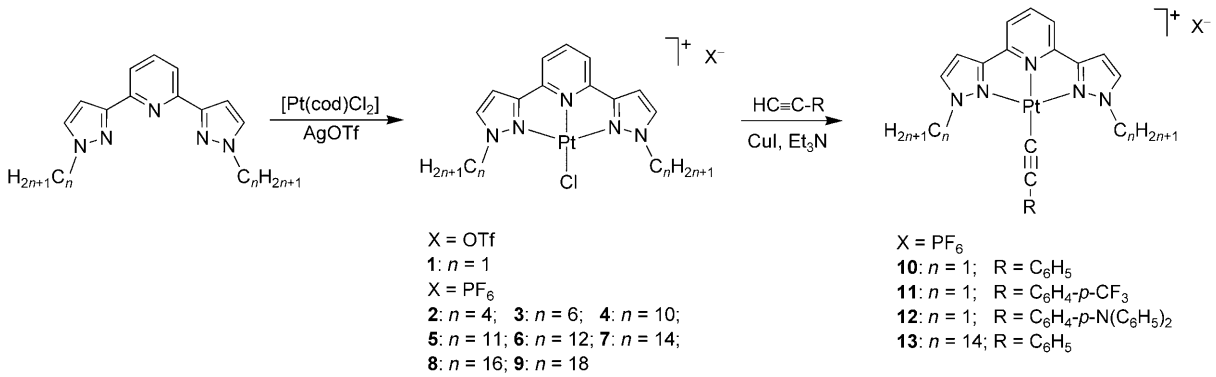

Scheme 1.

Results and Discussion

Synthesis and characterization: The 2,6-bis(1-alkylpyrazol-3-yl)-pyridine ligands were prepared by an alkylation reaction at the pyrazole N-1 position of 2,6-bis(pyrazol-3-yl)pyridine[15] with 1-bromoalkane or 1-iodoalkane. The chloroplatinum(II) (**1**–**9**) complexes were obtained by modifications of previously reported literature procedures for the synthesis of the related platinum(II) complexes.[7b] The alkynylplatinum(II) complexes (**10**–**13**) were synthesized by the reaction of the corresponding chloroplatinum(II) precursors with various organic alkynes in the presence of a catalytic amount of copper(I) iodide and triethylamine in dimethylformamide or dichloromethane (Scheme 1). The identities of all the complexes were fully established by performing ^{1}H NMR spectroscopy, fast atom bombardment (FAB) mass spectrometry and satisfactory elemental analyses. The crystal structures of **1**, **2**, and **10** have also been determined by X-ray crystallography.

Table 1. Selected bond lengths (Å) and angles (deg) for complexes **1**, **2**, and **10** with estimated standard deviations (esds) given in parentheses.

1		**2**		**10**	
bond lengths [Å]					
Pt(1)–N(2)	2.005(8)	Pt(1)–N(1)	1.964(4)	Pt(1)–N(2)	2.018(4)
Pt(1)–N(3)	1.961(8)	Pt(1)–N(2)	2.024(3)	Pt(1)–N(3)	1.994(4)
Pt(1)–N(4)	2.034(9)	Pt(1)–Cl(1)	2.297(2)	Pt(1)–N(4)	2.016(4)
Pt(1)–Cl(1)	2.288(3)	Pt(1)–Pt(1)	3.5001(8)	Pt(1)–C(14)	1.982(6)
Pt(2)–N(7)	1.982(11)			C(14)–C(14)	1.198(8)
Pt(2)–N(8)	1.928(12)			Pt(1)–Pt(1)	3.5886(6)
Pt(2)–N(9)	2.004(9)				
Pt(2)–Cl(2)	2.292(4)				
Pt(1)–Pt(2)	3.5583(10)				
bond angles [°]					
N(2)-Pt(1)-N(3)	79.0(3)	N(1)-Pt(1)-N(2)	79.02(8)	N(2)-Pt(1)-N(3)	78.85(15)
N(3)-Pt(1)-N(4)	78.3(3)	N(2)-Pt(1)-N(2*)	157.97(17)	N(3)-Pt(1)-N(4)	78.66(17)
N(2)-Pt(1)-N(4)	157.4(4)	N(1)-Pt(1)-Cl(1)	177.72(12)	N(2)-Pt(1)-N(4)	157.49(17)
N(3)-Pt(1)-Cl(1)	178.3(2)			N(3)-Pt(1)-C(14)	179.52(17)
N(7)-Pt(2)-N(8)	80.4(6)			Pt(1)-C(14)-C(15)	179.6(6)
N(8)-Pt(2)-N(9)	78.4(4)				
N(7)-Pt(2)-N(9)	158.8(6)				
N(8)-Pt(2)-Cl(2)	179.2(3)				

X-ray crystal structures: Single crystals of **1**, **2**, and **10** were obtained by slow diffusion of diethyl ether vapor into a solution of the respective complexes in acetonitrile and their structures were solved by X-ray crystallography. The perspective drawings of the complex cations of **1**, **2**, and **10** are shown in Figure 1. Selected bond distances and bond angles are tabulated in Table 1. All the structures show an essentially distorted square-planar coordination geometry, with bond parameters similar to those observed in typical platinum(II) terpyridyl complexes.[4,5,6f,8b,c] Due to the steric demand of the bis(pyrazol-3-yl)pyridine ligand, the N-Pt-N angles show deviations from the idealized values of 90° (78.3–80.4°) and 180° (157.4–158.8°). In each case, the platinum(II) metal center coordinates to the tridentate 2,6-bis(1-alkylpyrazol-3-yl)pyridine ligand through two pyrazolyl nitrogen atoms and one pyridyl nitrogen to form an essentially coplanar motif, whereas the Pt–N bond distances (1.96–2.03 Å) are similar to those found in other related platinum(II) terpyridyl or 2,6-bis(benzimidazol-2′-yl)pyridyl complexes.[4,5,6f,7,8b,c,10b] For **1** and **2**, the fourth coordination site is occupied by a chloro ligand with the Pt–Cl bond distances of 2.288–2.297 Å, which are comparable to those of the chloroplatinum(II) terpyridyl complexes.[4] For complex **10**, the remaining site is coordinated to an alkynyl ligand and the bond lengths of Pt–C and C≡C are 1.982 and 1.198 Å, respectively, which are comparable to those found in the related alkynylplatinum(II) complexes.[5,6f,7,8b,c] The interplanar angles between the phenyl ring of the alkynyl ligand and the 2,6-bis(1-alkylpyrazol-3-yl)pyridyl plane in **10** is about 21.19°. The observation of an essentially linear arrangement about the alkynyl group (N(3)-Pt(1)-C(14) 179.5°; Pt(1)-C(14)-C(15) 179.6°) is indicative of sp hybridization of the alkynyl carbon atoms.

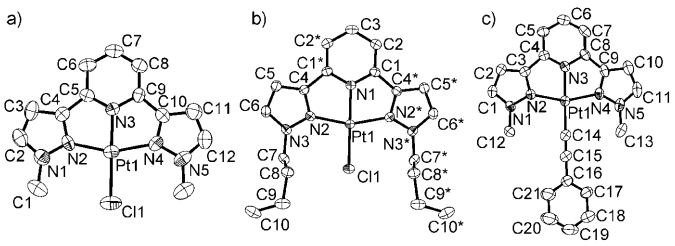

Figure 1. Perspective drawings of the complex cations of a) complex **1** (one of the independent molecules), b) complex **2**, and c) complex **10** with atomic numbering scheme. Hydrogen atoms and solvent molecules are omitted for clarity. Thermal ellipsoids are drawn at the 30% probability level.

The crystal packing of the complex cations of **1**, **2**, and **10** are depicted in Figure 2a–c, in which the molecules are packed with alternating "short" (3.558 Å **1**; 3.500 Å **2**; 3.587 Å **10**) and "long" Pt···Pt distances (4.193 Å **1**; 5.309 Å **2**; 4.503 Å **10**) in each case. It is noteworthy that their packing arrangements vary from one structure to another. For crystals **1** and **10** with the same tridentate ligand (N5C1), the complex cations are stacked into an extended columnar array with very small interplanar angles (0.974° **1**; 0–2.715° **10**) and short π–π separations (3.465 and 3.414 Å **1**; 3.458 and 3.484 Å **10**) between them. The [Pt(N5C1)] motifs are partially stacked with different extents of aromatic overlap from the head-to-tail or partial head-to-head configurations (Figure 2d and f). Although the [Pt(N5C1)] planes in the two complex cations with long Pt···Pt separation are laterally shifted, the observation of short interplanar distances sug-

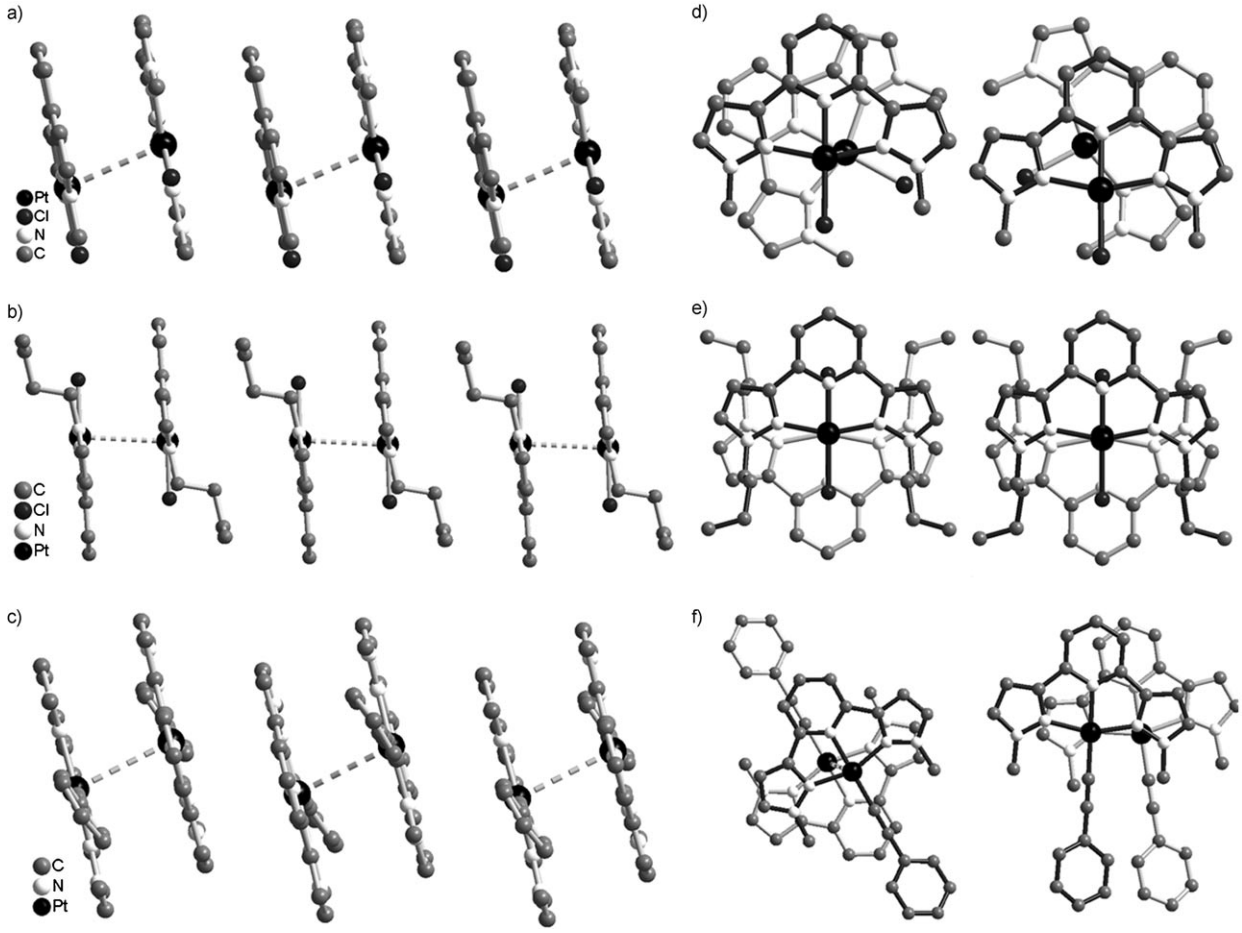

Figure 2. Crystal packing diagrams of the complex cations of a) complex **1**, b) complex **2**, and c) complex **10** showing the dimeric structure with alternating "short" and "long" Pt···Pt distances; and the views for various configurations of two complex cations of d) complex **1**, e) complex **2**, and f) complex **10**.

gests the presence of a weak intermolecular π–π bonding interaction amongst the molecules in their crystal lattices. On the other hand, the complex cations of **2** are stacked into pairs to form a dimeric structure, in which the [Pt(N5C4)] unit forms weak intermolecular Pt···Pt and π–π (interplanar distance of 3.474 Å) interactions with neighboring molecules. The crystal packing of **2** shows that the complex cations are arranged in a head-to-tail fashion without a lateral shift of the [Pt(N5C4)] motifs (Figure 2e), probably resulting from the minimization of the mutual repulsion between the sterically bulky butyl groups.

Electrochemistry: The cyclic voltammograms of the selected complexes in acetonitrile or dichloromethane (0.1 M nBu$_4$NPF$_6$) displayed two to three quasi-reversible couples at approximately −1.18 to −1.84 V and an irreversible anodic wave at approximately +0.84 to +2.11 V versus SCE. The electrochemical data for the selected complexes are summarized in Table 2, and the cyclic voltammograms for the oxidations of **1** and **10** in acetonitrile (0.1 M nBu$_4$NPF$_6$) are shown in Figure 3. The oxidation of chloroplatinum(II) complexes (**1**–**3** and **6**) was found to occur at almost the same potential of around +2.0 V versus SCE.

Table 2. Electrochemical data for selected complexes.[a]

Complex	Oxidation E_{pa} [V] vs. SCE[b]	Reduction $E_{1/2}$ [V] vs. SCE[c]
1	+1.95	−1.18, −1.57, −1.80
2	+2.05	−1.20, −1.64, −1.84
3	+2.11	−1.18, −1.63, −1.76
6[d]	+2.09	−1.20, −1.65
10	+1.57	−1.25, −1.40, −1.65
11	+1.68	−1.28, −1.42, −1.59
12	+0.84	−1.25, −1.42, −1.64
13[d]	+1.72	−1.24, −1.36, −1.67

[a] In acetonitrile with 0.1 M nBu$_4$NPF$_6$ (TBAH) as supporting electrolyte at room temperature; scan rate 100 mV s^{-1}. [b] E_{pa} refers to the anodic peak potential for the irreversible oxidation waves. [c] $E_{1/2}=(E_{pa}+E_{pc})/2$; E_{pa} and E_{pc} are peak anodic and peak cathodic potentials, respectively. [d] In acetonitrile–dichloromethane (2:1 v/v).

With reference to the previous studies on other platinum(II) complexes,[5a,d] this oxidation is assigned to metal-centered oxidation from Pt^{II} to Pt^{III}. In view of the observed change of the potentials for oxidation upon varying substituents on the alkynyl group, the oxidation in complexes **10**–**13** is assigned to the alkynyl-based ligand-centered oxidation, with substantial mixing of the platinum(II)-centered contribution. In general, the oxidation wave was found to occur at a more positive potential for the complexes with less electron-rich

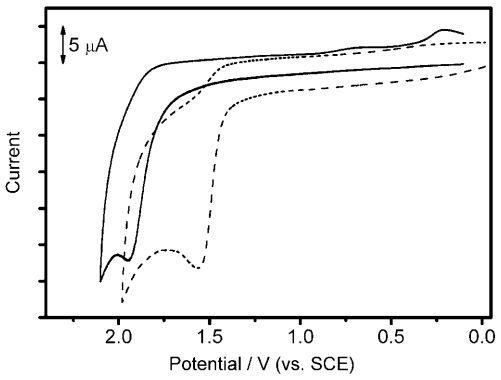

Figure 3. Cyclic voltammograms of **1** (——) and **10** (– – –) in CH_3CN ($0.1\ mol\,dm^{-3}\ nBu_4NPF_6$).

alkynyl ligands, such that **11** (+1.68 V) > **10** (+1.57 V) > **12** (+0.84 V), in line with the electron richness of the substituent on the ethynylbenzene ligand, $CF_3 < H < NPh_2$. On the basis of the similar potentials observed for the reduction couples for the complexes studied and the relative insensitivity of the potentials toward the nature of the alkynyl ligands with different substituents, the reduction couples are assigned to mainly arise from the ligand-centered reductions of the 2,6-bis(1-alkylpyrazol-3-yl)pyridine.

Electronic absorption spectroscopy: The electronic absorption spectra of complexes **1**–**13** in acetonitrile and/or dichloromethane at room temperature display high-energy absorption bands at 262–334 nm and moderately intense low-energy absorption bands at 356–482 nm. The photophysical data of **1**–**13** are summarized in Table 3. In view of the similar absorption bands observed in the 2,6-bis(1-alkylpyrazol-3-yl)pyridine (N5C*n*) ligands and alkynyes, the intense high-energy absorption bands, with extinction coefficients (ε) in the order of $10^4\ dm^3\,mol^{-1}\,cm^{-1}$, are attributed to intraligand (IL) π–π* transitions of the N5C*n* and alkynyl ligands (**10**–**13**). On the basis of the previous spectroscopic work on the related platinum(II) terpyridyl (trpy) and 2,6-bis(*N*-alkylbenzimidazol-2′-yl)pyridyl (bzimpy) complexes,[4–8] together with the absence of such low-energy absorptions in the N5C*n* ligand, the low-energy absorption band at 356–364 nm in the chloroplatinum(II) complexes **1**–**9**, with extinction coefficients (ε) in the order of $10^3\ dm^3\,mol^{-1}\,cm^{-1}$, is tentatively assigned as the (dπ(Pt)→π*(N5C*n*)) metal-to-ligand charge transfer (MLCT) transition. The occurrence of such low-energy absorption bands at similar energies indicates that variation of alkyl chain lengths on the pyrazolyl unit on the N5C*n* ligand would have little influence on the energy of the absorption. For the alkynylplatinum(II) complexes **10**–**13**, the low-energy absorption band at 368–482 nm is tentatively assigned to an admixture of (dπ(Pt)→π*(N5C*n*)) MLCT and (pπ(C≡C)→π*(N5C*n*)) ligand-to-ligand charge-transfer (LLCT) transition. Figure 4 shows the electronic absorption spectra of **1**, **10**, **11**, and **12**, in acetonitrile at room temperature. The red shift of the low-energy absorption in the alkynylplatinum(II) complexes **10**–**13**, relative to that of the chloroplatinum(II) complexes **1**–**9**, is ascribed to the greater destabilization of the HOMO derived from a filled–

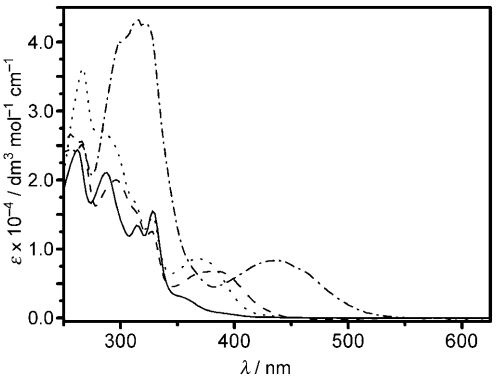

Figure 4. Electronic absorption spectra of **1** (——), **10** (– – –), **11** (·····), and **12** (–·–·) in CH_3CN at room temperature.

Table 3. Electronic absorption data for **1**–**13** at 298 K.

Complex	λ_{max} [nm] (ε_{max} [$dm^3\,mol^{-1}\,cm^{-1}$])	Medium
1	262 (24495), 288 (21060), 314 (13425), 328 (15515), 356 (2965)	CH_3CN
2	262 (22920), 288 (18710), 316 (11995), 330 (13875), 358 (2385)	CH_3CN
	266 (22840), 294 (19610), 318 (11480), 334 (13035), 364 (2465)	CH_2Cl_2
3	266 (26860), 294 (22435), 318 (13150), 334 (15210), 364 (3640)	CH_2Cl_2
4	266 (24640), 294 (19545), 318 (11125), 334 (12675), 364 (2325)	CH_2Cl_2
5	266 (24355), 294 (20520), 318 (11770), 334 (13560), 364 (2575)	CH_2Cl_2
6	264 (23890), 288 (19380), 316 (12180), 330 (14175), 358 (2570)	CH_3CN
	266 (23790), 294 (20425), 318 (11495), 334 (13005), 364 (2570)	CH_2Cl_2
7	266 (22720), 294 (19200), 318 (10885), 334 (12620), 364 (2230)	CH_2Cl_2
8	266 (23280), 294 (19720), 318 (11150), 334 (12890), 364 (2260)	CH_2Cl_2
9	266 (23820), 294 (20150), 318 (12080), 334 (13250), 364 (2375)	CH_2Cl_2
10	296 (20035), 314 (15345), 328 (12575), 386 (6810)	CH_3CN
	300 (22805), 328 (12645), 370 sh (6060), 406 (6030)	CH_2Cl_2
11	286 (27290), 312 (16960), 328 (14740), 368 (8585)	CH_3CN
12	298 (40055), 314 (43165), 324 (42500), 436 (8310)	CH_3CN
	302 (33360), 316 (34390), 328 (35860), 370 sh (7085), 482 (6185)	CH_2Cl_2
13	294 (19020), 314 (14140), 328 (12820), 366 sh (5145), 390 (4170)	CH_3CN
	300 (23000), 330 (14230), 370 sh (5820), 410 (3895)	CH_2Cl_2

filled pπ–dπ overlap as a result of the presence of the stronger σ- and π-donating alkynyl group. In general, the stronger the electron-donating ability of the alkynyl ligand is, the lower the energy of the lowest-energy absorption will be. The dependence of the absorption energy on the nature of the alkynyl ligand is in the order $R = CF_3 > H > NPh_2$, which is in line with the assignment of a transition of predominantly MLCT character with some mixing of a LLCT character.

Luminescence spectroscopy: No detectable emission was ob-

served for complexes **1**–**9** in acetonitrile or dichloromethane at room temperature, although a low-lying triplet (dπ(Pt)→π*(N5C*n*)) metal-to-ligand charge-transfer (^{3}MLCT) excited state is anticipated to exhibit luminescence behavior. A probable reason for the lack of luminescence behavior is the presence of low-energy d–d ligand field (LF) states, which would quench the ^{3}MLCT state by the thermally accessible ^{3}d–d excited state by nonradiative decay. A similar observation has been reported in the related platinum(II) terpyridyl systems.[4] On the contrary, the alkynylplatinum(II) complexes **10** and **11** were found to exhibit luminescence at about 540 nm in acetonitrile at 298 K (Figure 5, Table 4).

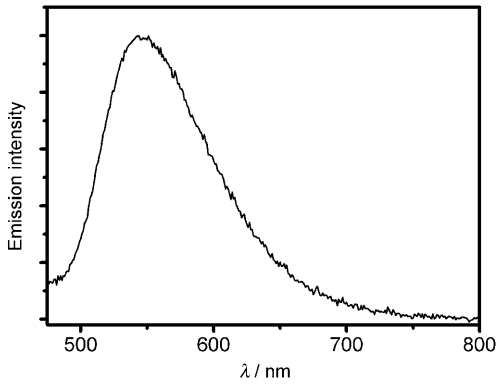

Figure 5. Emission spectrum of **10** in CH_3CN at room temperature.

Table 4. Luminescence data for **10**–**13**.

Complex	Emission medium (T [K])	λ_{max} [nm] (τ_o [μs])
10	CH_3CN (298)[a]	545 (1.38)
	Solid (298)	605 (<0.1)
	Solid (77)	590 (1.58)
11	CH_3CN (298)[a]	540 (1.50)
	Solid (298)	550 (<0.1)
	Solid (77)	578 (3.70)
12	CH_3CN (298)[a]	–[b]
	Solid (298)	662 (<0.1)
	Solid (77)	630 (1.14)
13	CH_3CN (298)	–[b]
	Solid (298)	530 (<0.1)
	LB film (298)	690

[a] Sample concentration in the range of $4.0–6.3\times10^{-5}$ M. [b] Nonemissive.

The large Stokes shifts and observed lifetimes in the microsecond range for their emissions are suggestive of an origin of triplet parentage. With reference to the previous spectroscopic studies of other related alkynylplatinum(II) terpyridyl or 2,6-bis(benzimidazol-2′-yl)pyridyl complexes, an emission origin of a (dπ(Pt)→π*(N5C*n*)) ^{3}MLCT excited state, with some mixing of a (pπ(C≡C)→π*(N5C*n*)) ^{3}LLCT character, is assigned. The observation of the emission band of **11** at higher energy than **10** is in line with a ^{3}MLCT/LLCT excited state origin assignment, since the presence of the electron-deficient trifluoromethyl group on the phenyl ring of the alkynyl unit would render the HOMO lower lying in energy, leading to a higher energy MLCT/LLCT emission. Complex **12**, with the strongly electron-donating amino substituents on the phenyl ring of the alkynyl ligand was found to be nonemissive in acetonitrile at 298 K. The lack of emissive behavior in **12** may be ascribed to the quenching of the emissive state by photoinduced electron transfer (PET), in which the electron is transferred from the electron-rich amino group to the platinum(II) 2,6-bis(1-methylpyrazol-3-yl)pyridyl moiety to quench the emissive ^{3}MLCT excited state. The quenching of the ^{3}MLCT excited state could also be rationalized by the presence of an energetically accessible or lower-lying nonemissive ^{3}LLCT excited state, as a result of a relatively higher-lying pπ(C≡CR) orbital due to the presence of the electron-donating amino substituent. Similar nonemissive behavior has been observed in the related platinum(II) terpyridyl complexes with electron-donating methoxy or amino substituents on the phenyl ring of the alkynyl group.[5,8a,b] All the alkynylplatinum(II) complexes **10**–**13** exhibit an intense emission in the solid state at 298 and 77 K. Similar to the electronic absorption studies, the solid-state emission energies of the complexes were found to depend on the nature of the substituents on the phenyl ring of the alkynyl ligands, in such a trend that the stronger the electron-donating ability of the alkynyl ligand is, the lower the emission energy will be (Figure 6).

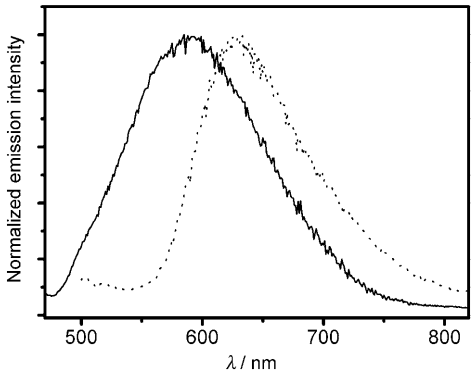

Figure 6. Solid state emission spectra of **10** (——) and **12** (·····) at 77 K.

Langmuir–Blodgett films: To investigate the amphiphilic properties, complexes **7** and **13**, containing two long alkyl chains of $C_{14}H_{29}$ on the pyrazolyl units, were subjected to Langmuir–Blodgett film formation studies. Figure 7 shows the surface pressure–molecular area (π–A) isotherm of **7** and **13**. The π–A isotherms of **7** and **13** show one well-defined condensed region with collapse pressures of 40–45 mN m^{-1}, indicative of the good and stable air–water interface behavior of the complexes. It is worth noting that these complexes have similar π–A isotherms with fairly high collapse pressures as a result of the similarity in their structures. By extrapolating the plot in the condensed region to zero pressure, the limiting molecular areas of 0.63 and 0.71 nm^2 are estimated for complexes **7** and **13**, respectively. In view of this, together with the observation of a very steep

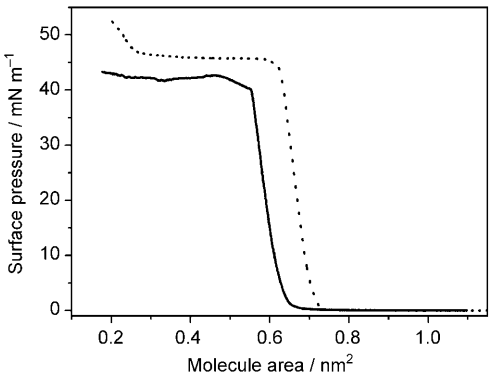

Figure 7. Surface pressure–molecular area isotherm of **7** (——) and **13** (•••••) on a pure water subphase at 20°.

isotherm, it is suggested that the molecules are rather compactly packed in the film and the coordination planes are stacked adjacent to each other with the long alkyl chains vertically oriented with respect to the water surface in an "edge-on" orientation rather than a "flat-on" arrangement.

Multilayer LB films of **7** and **13** were successfully prepared onto the glass substrates by using the Y-type deposition method. The transfer ratios in both the dipping and the lifting processes were constant and were almost the same, approaching unity. Since small-angle XRD is a useful tool to estimate the molecular ordering, as well as the molecular orientation in LB films on solid substrates, small-angle XRD was performed on a 47-layer Y-type LB film of **7** prepared at 35 mN m^{-1}. Third-order diffractions were observed in the XRD patterns of the LB film at 20 °C (Figure 8a), indicating a well-organized layered structure. A sharp (001) Bragg diffraction was observed at $2\theta = 2.62°$ and a layer distance (d spacing) of 3.4 nm was calculated by the Bragg's equation. Such a value further supports an edge-on orientation with the long alkyl chains tilted away from the normal of the glass substrate after the transfer. Figure 8b–e shows the X-ray photoelectron spectroscopy (XPS) core level spectra for the 47-layer LB film of **7** transferred at 35 mN m^{-1} on a quartz plate. The XPS wide-scan spectrum showed characteristic elemental signatures for C 1s, Pt 4f, N ls, P 2p, Cl 2p, and F 1s lines, which are in good agreement with the chemical formula of **7**. In the high-resolution spectra, the Pt $4f_{5/2}$ and Pt $4f_{7/2}$ signals were observed at 76.9 and 73.6 eV, respectively, which are typical values for platinum(II) complexes. Angular-resolved Pt 4f, Cl 2p, and N 1s spectra showed little angular dependence, which gives additional support for the edge-on orientation of **7** in the LB films deposited on the hydrophilic glass substrate.

The deposition process onto a quartz plate of the LB film was monitored by UV/Vis spectroscopy. The absorbance was found to increase linearly with an increase in the number of deposition layers. The electronic absorption spectra of **7** in LB films as a function of layer number are shown in Figure 9a. A linear relationship between the absorbance at 256 nm and the number of layers deposited on the quartz substrate was obtained, which was indicative of the good film formation behavior of the complex to form stable and uniform LB films. The absorption patterns of the LB films of **7** (257, 295, 321, 338, and 373 nm) and **13** (259, 303, 335, and 393 nm), are found to occur at similar energies to the corresponding complexes found in fluid solution. Notably, a low-energy emission band at 693 nm was observed in the 47-layer LB film of **13** (Figure 9b). The red shift in emission energy of **13** in the 47-layer LB films relative to that in the solid state at room temperature (530 nm), is suggestive of the increased extent of Pt···Pt interactions and/or π–π stacking in the LB film as a result of the close molecular packing in the ordered arrangement, as revealed by the LB film characterization in the π–A isotherm and XRD pattern. The origin of these low-energy emission bands is tentatively assigned as metal-metal-to-ligand charge-transfer (MMLCT) and excimeric emissions derived from the stacking of the platinum(II) 2,6-bis(1-tetradecylpyrazol-3-yl)pyridyl moieties in the LB film, similar to that observed in J-aggregate formation which enhances the molecular interaction, and will be further described by using a proposed model (see below).

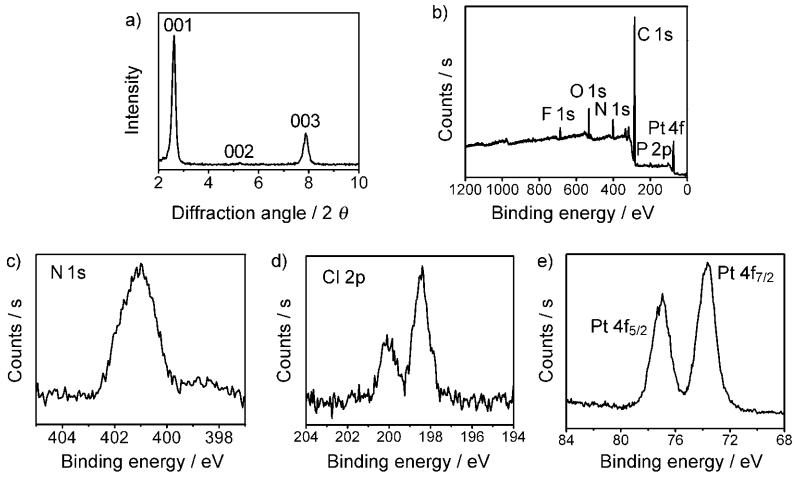

Figure 8. a) XRD patterns of a 47-layer LB film of **7** transferred at the surface pressure of 35 mN m^{-1} at 20 °C; b) XPS wide-scan spectrum for a 47-layer LB film of **7** on a quartz plate transferred at 35 mN m^{-1}, and c)–d) high-resolution spectra in the N 1s, Cl 2p, and Pt 4f regions.

To provide further structural information based on the sensitivity of the vibrational modes to the molecular structure and dynamics of the alkyl chains,[16] FTIR spectroscopy was employed to probe the structure of the multilayer LB film of **7** at room temperature. As shown in Figure 10a, the absorption bands at 2919 and 2850 cm^{-1} are assigned to the antisymmetric (d^-) and symmetric (d^+) stretching vibrations of the ethylene group, respectively. It is well known that the d^- and d^+

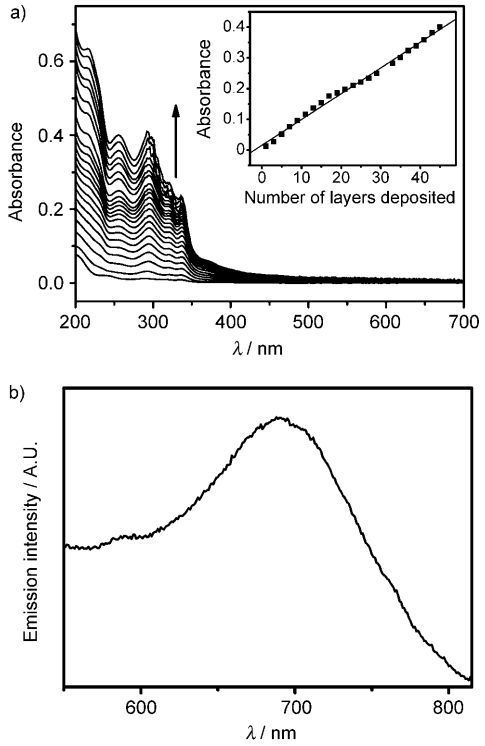

Figure 9. a) UV/Vis absorption spectra of the LB film of **7** with different numbers of layers deposited on a quartz plate at a surface pressure of 35 mN m^{-1} (from bottom to top: 1–45 layers with intervals of 2 layers). The inset shows the absorbance at 256 nm as a function of layer number. b) Emission spectrum of a 47-layer LB-film of **13**.

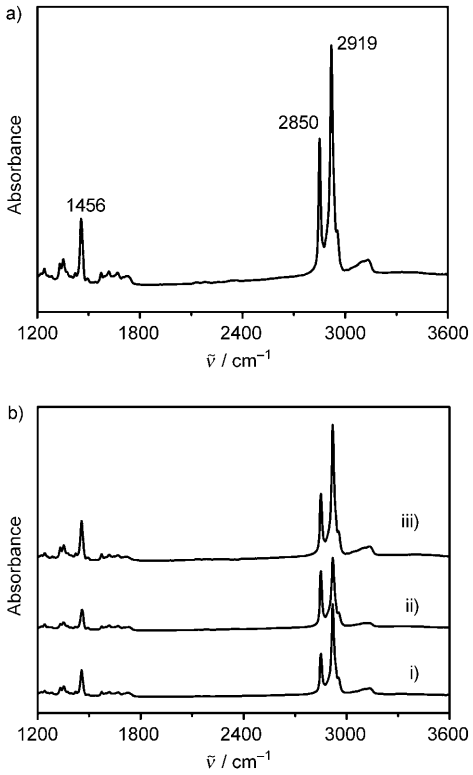

Figure 10. a) IR spectra of an 82-layer LB film of **7** on a CaF_2 plate transferred at 35 mN m^{-1} at 20 °C; b) Polarized infrared spectra of an 82-layer LB film of **7** on a CaF_2 plate transferred at 35 mN m^{-1} at 20 °C with the incident angles of i) $\measuredangle_{\parallel}$ (i = 0°), ii) $\measuredangle_{\perp}$ (i = 0°), and iii) $\measuredangle_{\parallel}$ (i = 60°), respectively.

bands are strong indicators of the chain conformation, in which low frequencies (2915–2920 and 2846–2850 cm^{-1}) of the bands are characteristic of highly ordered alkyl chains,[17] whereas shifts to higher frequencies (2924–2928 and 2854–2856 cm^{-1}) are indicative of an increase in gauche conformers, with the alkyl chain conformation tending towards disorder. Accordingly, the observed absorptions at 2919 and 2850 cm^{-1} reveal the presence of highly ordered alkyl chains, whereas the absorption band at 1456 cm^{-1} is typical of the CH_2 scissoring bending mode, which is widely employed for the diagnosis of alkyl chain packing.[18] Based on the IR absorption study,[19] the molecular orientation in the thin film can be determined. The calculated mean tilting angle of the alkyl chains has been determined to be about 25°, based on the linear relationship of the diagnostic bands (Figure 10b). In view of the fact that the LB film was prepared in Y-type, one can assume that the alkyl chains would form a bilayer arrangement on each side of the coordination planes. With a length of 1.8 nm estimated from an ideal all-*trans* conformation of the alkyl chains, a calculated thickness for the sandwich layer of about 3.2 nm would be obtained. Since the length of the Pt chromophoric plane given by the X-ray crystal structure of **2** is found to be 1.02 nm, it is likely that there would only be a very small angle between the Pt plane and the substrate. Thus, the calculated thickness of about 3.2 nm, which is essentially almost similar to the length of the alkyl chains in the bilayer, is in good agreement with the layer thickness of 3.4 nm obtained from the XRD measurement. Based on these structural properties, a possible packing model of the LB film is proposed as shown in Figure 11.

According to the X-ray structure of **2**, the area of the Pt chromophoric plane can be estimated to be about 0.64 nm^2. Considering the small angle between the Pt chromophoric plane and the substrate, the estimated area could approxi-

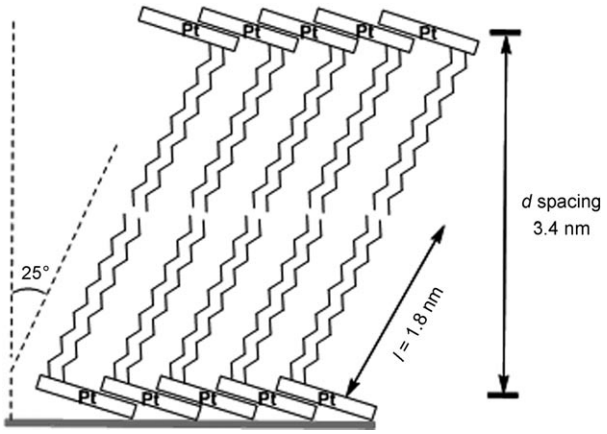

Figure 11. Schematic representation showing the proposed packing structure of a LB film of **7**.

mately be taken to be equal to the projected area. This estimated area is in good agreement with the limiting molecular area of 0.63 nm^2 obtained from the π–A isotherm, providing further support for the proposed packing model of the LB film.

Conclusion

Two series of novel chloroplatinum(II) and alkynylplatinum(II) complexes, [Pt(N5C*n*)Cl][X] (**1–9**) and [Pt(N5C*n*)-(C≡CR)][X] (**10–13**) (X = OTf or PF_6; R = C_6H_5, C_6H_4-*p*-CF_3 and C_6H_4-*p*-N(C_6H_5)$_2$), with a new type of tridentate ligand, 2,6-bis(1-alkylpyrazol-3-yl)pyridyl (N5C*n*), with various chain lengths of the alkyl groups on the nitrogen atom of the pyrazolyl units, have been successfully synthesized and characterized. Their electrochemical and photophysical properties have been studied. Molecular structures of **1**, **2**, and **10** have also been determined by X-ray crystallography, in which the molecules are packed with alternating "short" (3.558 Å **1**; 3.500 Å **2**; 3.587 Å **10**) and "long" Pt···Pt distances (4.193 Å **1**; 5.309 Å **2**; 4.503 Å **10**) in each case. [Pt(N5C14)Cl]PF_6 (**7**) and [Pt(N5C14)(C≡CC_6H_5)]PF_6 (**13**), with two amphiphilic tetradecyl groups on the nitrogen atom of the pyrazolyl units, were found to form stable and reproducible LB films at the air–water interface. The characterization of such LB films has been investigated by the study of their surface pressure–area (π–A) isotherms, UV/Vis spectroscopy, XRD, X-ray photoelectron spectroscopy (XPS), IR and polarized IR spectroscopy. A 47-layer LB film of **13** was found to exhibit a low-energy emission band at 693 nm, which is indicative of the presence of Pt···Pt interactions and/or π–π stacking as a result of the close molecular packing in the ordered arrangement, as revealed by the LB film characterization in the π–A isotherm and XRD pattern. The origin of these low-energy emission bands is tentatively assigned as metal-metal-to-ligand charge-transfer (MMLCT) and excimeric emissions derived from the stacking of the platinum(II) 2,6-bis(1-tetradecylpyrazol-3-yl)pyridyl moieties in the LB film.

Experimental Section

Materials and reagents: Dichloro(1,5-cyclooctadiene)platinum(II), phenylacetylene, and 4-trifluorophenylacetylene were purchased from Aldrich Chemical Co. Iodomethane, 1-bromobutane, 1-bromohexane, 1-bromodecane, 1-bromoundecane, 1-bromododecane, 1-bromotetradecane, 1-iodohexadecane, and ammonium hexafluorophosphate were obtained from Alfa Aesar. Sodium hydride was purchased from Tian Tai Chemical Co. 2,6-Diacetylpyridine, 2,6-bis(pyrazol-3-yl)pyridine,[15] and 4-ethynylphenyldiphenylamine[20] were synthesized according to modifications of the methods described in the literature. Analytical grade chloroform was used as a spreading solvent and was distilled before use. Pure water (Milli-Pore; 18.2 MΩcm) was employed for LB film deposition experiments. All solvents and other reagents were of analytical grade and were used as received.

2,6-bis(1-methylpyrazol-3-yl)pyridine (N5C1): A mixture of 2,6-bis(pyrazol-3-yl)pyridine (500 mg, 2.3 mmol), iodomethane (1 mL, 16 mmol) and sodium hydride (380 mg, 60%, 9.5 mmol) in 30 mL dry DMF was heated to reflux for 2 days. The solvent was removed under vacuum and the mixture was washed with distilled water and extracted with chloroform (3× 30 mL). After evaporation of the solvent, the product was purified by column chromatography on silica gel with chloroform–methanol (20:1 v/v) as eluent to give the desired product as a white solid. Yield: 338 mg, 60%. ^{1}H NMR (500 MHz, $CDCl_3$, 298 K, relative to Me_4Si): δ = 3.99 (s, 6H; -CH_3), 7.00 (d, J = 2.3 Hz, 2H; pyrazolyl protons), 7.41 (d, J = 2.3 Hz, 2H; pyrazolyl protons), 7.73 (t, J = 7.8 Hz, 1H; pyridyl proton), 7.85 ppm (d, J = 7.8 Hz, 2H; pyridyl proton); MS (EI$^+$): m/z: 263 [M+Na]$^+$; elemental analysis calcd (%) for $C_{13}H_{13}N_5$: C 65.25, H 5.48, N 29.27; found: C 65.43 H 5.61, N 29.09.

2,6-bis(1-butylpyrazol-3-yl)pyridine (N5C4): The procedure was similar to that for N5C1 except that 1-bromobutane (1 mL, 9.2 mmol) was used in place of iodomethane to give a yellow oil. Yield: 535 mg, 70%. ^{1}H NMR (500 MHz, $CDCl_3$, 298 K, relative to Me_4Si): δ = 0.95 (t, J = 7.4 Hz, 6H; -CH_3), 1.33–1.40 (m, 4H; -CH_2-CH_3), 1.86–1.92 (m, 4H; -CH_2-CH_2-CH_3), 4.18 (t, J = 7.2 Hz, 4H; -CH_2-(CH_2)$_2$-CH_3), 7.00 (d, J = 2.2 Hz, 2H; pyrazolyl protons), 7.42 (d, J = 2.2 Hz, 2H; pyrazolyl protons), 7.72 (t, J = 7.8 Hz, 1H; pyridyl proton), 7.86 ppm (d, J = 7.8 Hz, 2H; pyridyl protons); MS (EI$^+$): m/z: 347 [M+Na]$^+$; elemental analysis calcd (%) for $C_{19}H_{25}N_5$: C 70.56, H 7.79, N 21.65; found: C 70.12, H 8.15, N 21.37.

2,6-bis(1-hexylpyrazol-3-yl)pyridine (N5C6): The procedure was similar to that for N5C1 except that 1-bromohexane (1.5 mL, 9.1 mmol) was used in place of iodomethane to give a yellow oil. Yield: 610 mg, 68%. ^{1}H NMR (500 MHz, $CDCl_3$, 298 K, relative to Me_4Si): δ = 0.88 (t, J = 6.8 Hz, 6H; -CH_3), 1.26–1.35 (m, 12H; -(CH_2)$_3$-CH_3), 1.88–1.94 (m, 4H; -CH_2-(CH_2)$_3$-CH_3), 4.17 (t, J = 7.2 Hz, 4H; -CH_2-(CH_2)$_4$-CH_3), 7.00 (d, J = 2.2 Hz, 2H; pyrazolyl protons), 7.42 (d, J = 2.2 Hz, 2H; pyrazolyl protons), 7.73 (t, J = 7.7 Hz, H; pyridyl proton), 7.86 ppm (d, J = 7.7 Hz, 2H; pyridyl protons); MS (EI$^+$): m/z: 403 [M+Na]$^+$; elemental analysis calcd (%) for $C_{23}H_{33}N_5$: C 72.78, H 8.76, N 18.45; found: C 72.44, H 8.98, N 18.01.

2,6-bis(1-decylpyrazol-3-yl)pyridine (N5C10): The procedure was similar to that for N5C1 except that 1-bromodecane (2 mL, 9.6 mmol) was used in place of iodomethane to give a yellow oil. Yield: 755 mg, 65%. ^{1}H NMR (500 MHz, $CDCl_3$, 298 K, relative to Me_4Si): δ = 0.88 (t, J = 6.8 Hz, 6H; -CH_3), 1.25–1.32 (m, 28H; -(CH_2)$_7$-CH_3), 1.89–1.92 (m, 4H; -CH_2-(CH_2)$_7$-CH_3), 4.17 (t, J = 7.2 Hz, 4H; -CH_2-(CH_2)$_8$-CH_3), 6.99 (d, J = 2.2 Hz, 2H; pyrazolyl protons), 7.42 (d, J = 2.2 Hz, 2H; pyrazolyl protons), 7.72 (t, J = 7.8 Hz, 1H; pyridyl proton), 7.86 ppm (d, J = 7.8 Hz, 2H; pyridyl protons); MS (EI$^+$): m/z: 515 [M+Na]$^+$; elemental analysis calcd (%) for $C_{31}H_{49}N_5$: C 75.71, H 10.04, N 14.24; found: C 75.60, H 10.39, N 14.52.

2,6-bis(1-undecylpyrazol-3-yl)pyridine (N5C11): The procedure was similar to that for N5C1 except that 1-bromoundecane (2 mL, 8.9 mmol) was used in place of iodomethane to give a yellow oil. Yield: 737 mg, 60%. ^{1}H NMR (500 MHz, $CDCl_3$, 298 K, relative to Me_4Si): δ = 0.87 (t, J = 6.8 Hz, 6H; -CH_3), 1.25–1.32 (m, 32H; -(CH_2)$_8$-CH_3), 1.89–1.92 (m, 4H; -CH_2-(CH_2)$_8$-CH_3), 4.17 (t, J = 7.2 Hz, 4H; -CH_2-(CH_2)$_9$-CH_3), 7.00 (d, J = 2.2 Hz, 2H; pyrazolyl protons), 7.42 (d, J = 2.2 Hz, 2H; pyrazolyl protons), 7.72 (t, J = 7.8 Hz, 1H; pyridyl proton), 7.86 ppm (d, J = 7.8 Hz, 2H; pyridyl protons); MS (EI$^+$): m/z: 543 [M+Na]$^+$; elemental analysis calcd (%) for $C_{33}H_{53}N_5$: C 76.25, H 10.28, N 13.47; found: C 76.55, H 10.68, N 13.37.

2,6-bis(1-dodecylpyrazol-3-yl)pyridine (N5C12): The procedure was similar to that for N5C1 except that 1-bromododecane (2 mL, 8.9 mmol) was used in place of iodomethane to give a yellow oil. Yield: 830 mg, 64%. ^{1}H NMR (400 MHz, $CDCl_3$, 298 K, relative to Me_4Si): δ = 0.87 (t, J = 6.3 Hz, 6H; -CH_3), 1.25–1.32 (m, 36H; -(CH_2)$_9$-CH_3), 1.89–1.92 (m, 4H; -CH_2-(CH_2)$_9$-CH_3), 4.16 (t, J = 7.2 Hz, 4H; -CH_2-(CH_2)$_{10}$-CH_3), 6.99 (d, J = 2.2 Hz, 2H; pyrazolyl protons), 7.42 (d, J = 2.2 Hz, 2H; pyrazolyl protons), 7.72 (t, J = 7.7 Hz, 1H; pyridyl proton), 7.86 ppm (d, J = 7.7 Hz, 2H; pyridyl protons,); MS (EI$^+$): m/z: 571 [M+Na]$^+$; elemental analysis calcd (%) for $C_{35}H_{57}N_5$: C 76.73, H 10.49, N 12.78; found: C 76.35, H 10.81, N 12.54.

2,6-bis(1-tetradecylpyrazol-3-yl)pyridine (N5C14): The procedure was similar to that for N5C1 except that 1-bromotetradecane (2 mL, 7.3 mmol) was used in place of iodomethane to give a white solid. Yield: 913 mg, 64%. ^{1}H NMR (400 MHz, $CDCl_3$, 298 K, relative to Me_4Si): $\delta =$ 0.87 (t, $J=6.2$ Hz, 6H; -CH_3), 1.25–1.32 (m, 44H, -$(CH_2)_{11}$-CH_3), 1.89–1.93 (m, 4H; -CH_2-$(CH_2)_{11}$-CH_3), 4.16 (t, $J=7.2$ Hz, 4H; -CH_2-$(CH_2)_{12}$-CH_3), 6.99 (d, $J=2.1$ Hz, 2H; pyrazolyl protons), 7.42 (d, $J=2.1$ Hz, 2H; pyrazolyl protons,), 7.72 (t, $J=7.6$ Hz, 1H; pyridyl proton), 7.86 ppm (d, $J=7.6$ Hz, 2H; pyridyl protons); MS (EI$^+$): m/z: 627 $[M+Na]^+$; elemental analysis calcd (%) for $C_{39}H_{65}N_5$: C 77.56, H 10.85, N 11.60; found: C 77.29, H 10.36, N 11.10.

2,6-bis(1-hexadecylpyrazol-3-yl)pyridine (N5C16): The procedure was similar to that for N5C1 except that 1-iodohexadecane (3.3 g, 9.5 mmol) was used in place of iodomethane to give a white solid. Yield: 904 mg, 58%. ^{1}H NMR (400 MHz, $CDCl_3$, 298 K, relative to Me_4Si): $\delta=0.87$ (t, $J=5.3$ Hz, 6H; -CH_3), 1.25–1.32 (m, 52H; -$(CH_2)_{13}$-CH_3), 1.89–1.92 (m, 4H; -CH_2-$(CH_2)_{13}$-CH_3), 4.16 (t, $J=7.0$ Hz, 4H; -CH_2-$(CH_2)_{14}$-CH_3), 6.99 (d, $J=1.4$H, 2H; pyrazolyl protons), 7.42 (d, $J=1.4$ Hz, 2H; pyrazolyl protons), 7.72 (t, $J=7.8$ Hz, 1H; pyridyl proton), 7.86 ppm (d, $J=7.8$ Hz, 2H; pyridyl protons); MS (EI$^+$): m/z: 683 $[M+Na]^+$; elemental analysis calcd (%) for $C_{43}H_{73}N_5$: C 78.30, H 11.08, N 10.62; found: C 78.34, H 10.58, N 10.22.

2,6-bis(1-octadecylpyrazol-3-yl)pyridine (N5C18): The procedure was similar to that for N5C1 except that 1-bromooctadecane (3.1 g, 9.5 mmol) was used in place of iodomethane to give a white solid. Yield: 846 mg, 50%. ^{1}H NMR (400 MHz, $CDCl_3$, 298 K, relative to Me_4Si): $\delta=0.85$ (t, $J=6.8$ Hz, 6H; -CH_3), 1.25–1.32 (m, 60H; -$(CH_2)_{15}$-CH_3), 1.89–1.93 (m, 4H; -CH_2-$(CH_2)_{15}$-CH_3), 4.17 (t, $J=7.2$ Hz, 4H; -CH_2-$(CH_2)_{16}$-CH_3), 7.00 (d, $J=2.3$ Hz, 2H; pyrazolyl protons), 7.42 (d, $J=2.3$ Hz, 2H; pyrazolyl protons), 7.72 (t, $J=7.7$ Hz, 1H, pyridyl proton), 7.86 ppm (d, $J=7.7$ Hz, 2H, pyridyl protons); MS (EI$^+$): m/z: 739 $[M+Na]^+$; elemental analysis calcd (%) for $C_{47}H_{81}N_5$: C 78.82, H 11.40, N 9.78; found: C 79.14, H 11.28, N 9.58.

[Pt(N5C1)Cl]OTf (1): A mixture of dichloro(1,5-cyclooctadiene)platinum(II) (140 mg, 0.37 mmol) and N5C1 (98 mg, 0.41 mmol) was heated to reflux in acetone–acetonitrile (2:1 v/v) for 2 days. After evaporation of the solvent, the residue was washed with diethyl ether to give a pale yellow solid. Recrystallization from vapor diffusion of diethyl ether into a methanol–acetonitrile (1:1 v/v) solution mixture of the product gave **1** as yellow crystals. Yield: 69 mg, 30%. ^{1}H NMR (500 MHz, $[D_6]$DMSO, 298 K, relative to Me_4Si): $\delta=4.13$ (s, 6H, -CH_3), 7.31 (d, $J=7.7$ Hz, 2H; pyrazolyl protons), 8.08 (d, $J=7.7$ Hz, 2H; pyrazolyl protons), 8.23 (d, $J=7.8$ Hz, 2H; pyridyl protons), 8.36 ppm (t, $J=7.8$ Hz, 1H; pyridyl proton); MS (FAB$^+$): m/z: 471 $[M-OTf]^+$; elemental analysis calcd (%) for $C_{14}H_{13}N_5ClSO_3F_3Pt$·MeOH: C 27.67, H 2.31, N 10.76; found: C 27.67, H 2.04, N 10.67.

[Pt(N5C4)Cl]PF_6 (2): A mixture of dichloro(1,5-cyclooctadiene)platinum(II) (140 mg, 0.37 mmol) and N5C4 (132 mg, 0.41 mmol) was heat to reflux in acetone–acetonitrile (2:1 v/v) for 2 days. After evaporation of the solvent, the residue was washed with diethyl ether. A pale yellow solid was obtained, which was then dissolved in a minimum amount of methanol, followed by a metathesis reaction to the hexafluorophosphate salt by using ammonium hexafluorophosphate. Subsequent recrystallization by vapor diffusion of diethyl ether into a solution of the product in acetonitrile gave **2** as pale yellow crystals. Yield: 116 mg, 45%. ^{1}H NMR (500 MHz, $CDCl_3$, 298 K, relative to Me_4Si): $\delta=0.99$ (t, $J=7.4$ Hz, 6H; -CH_3), 1.33–1.40 (m, 4H; -CH_2-CH_3), 1.86–1.92 (m, 4H; -CH_2-CH_2-CH_3), 4.74 (t, $J=7.4$ Hz, 4H; -CH_2-$(CH_2)_2$-CH_3), 7.08 (d, $J=2.9$ Hz, 2H; pyrazolyl protons), 7.68 (d, $J=2.9$ Hz, 2H; pyrazolyl protons), 7.70 (d, $J=8.0$ Hz, 2H; pyridyl protons), 8.27 ppm (t, $J=8.0$ Hz, 1H; pyridyl protons); MS (FAB$^+$): m/z: 555 $[M-PF_6]^+$; elemental analysis calcd (%) for $C_{19}H_{25}N_5ClPF_6Pt$·1/4CH_3CN: C 33.04, H 3.35, N 10.38; found: C 33.09, H 3.55, N 10.37.

[Pt(N5C6)Cl]PF_6 (3): The procedure was similar to that for **2** except that N5C6 (155 mg, 0.41 mmol) was used in place of N5C4 to give **3** as a pale yellow solid. Yield: 126 mg, 45%. ^{1}H NMR (500 MHz, $CDCl_3$, 298 K, relative to Me_4Si): $\delta=0.88$ (t, $J=6.9$ Hz, 6H; -CH_3), 1.25–1.36 (m, 12H; -$(CH_2)_3$-CH_3), 1.88–1.94 (m, 4H; -CH_2-$(CH_2)_3$-CH_3), 4.68 (t, $J=7.5$ Hz, 4H; -CH_2-$(CH_2)_4$-CH_3), 7.04 (d, $J=2.9$ Hz, 2H; pyrazolyl protons), 7.71 (d, $J=2.9$ Hz, 2H; pyrazolyl protons), 7.86 (d, $J=8.0$ Hz, 2H; pyridyl protons), 8.22 ppm (t, $J=8.0$ Hz, 1H; pyridyl proton); MS (FAB$^+$): m/z: 611 $[M-PF_6]^+$; elemental analysis calcd (%) for $C_{23}H_{33}N_5ClPF_6Pt$·1/4CH_3CN: C 36.85, H 4.41, N 9.60; found: C 37.11, H 4.45, N 9.35.

[Pt(N5C10)Cl]PF_6 (4): The procedure was similar to that for **2** except that N5C10 (201 mg, 0.41 mmol) was used in place of N5C4. Subsequent recrystallization by vapor diffusion of diethyl ether into a solution of the product in dichloromethane gave **4** as a pale yellow solid. Yield: 138 mg, 43%. ^{1}H NMR (500 MHz, $CDCl_3$, 298 K, relative to Me_4Si): $\delta=0.86$ (t, $J=6.9$ Hz, 6H; -CH_3), 1.21–1.32 (m, 28H; -$(CH_2)_7$-CH_3), 1.89–1.92 (m, 4H; -CH_2-$(CH_2)_7$-CH_3), 4.66 (t, $J=7.4$ Hz, 4H; -CH_2-$(CH_2)_8$-CH_3), 7.03 (d, $J=2.8$ Hz, 2H; pyrazolyl protons), 7.72 (d, $J=2.8$ Hz, 2H; pyrazolyl protons), 7.84 (d, $J=8.0$ Hz, 2H; pyridyl protons), 8.19 ppm (t, $J=$ 8.0 Hz, 1H, pyridyl proton); MS (FAB$^+$): m/z: 723 $[M-PF_6]^+$; elemental analysis calcd (%) for $C_{31}H_{49}N_5ClPF_6Pt$: C 42.93, H 5.69, N 8.08; found: C 43.28, H 5.97, N 8.04.

[Pt(N5C11)Cl]PF_6 (5): The procedure was similar to that for **2** except that N5C11 (213 mg, 0.41 mmol) was used in place of N5C4. Subsequent recrystallization by vapor diffusion of diethyl ether into a solution of the product in dichloromethane gave **5** as a pale yellow solid. Yield: 116 mg, 35%. ^{1}H NMR (500 MHz, $CDCl_3$, 298 K, relative to Me_4Si): $\delta=0.87$ (t, $J=6.9$ Hz, 6H; -CH_3), 1.25–1.33 (m, 32H; -$(CH_2)_8$-CH_3), 1.89–1.92 (m, 4H; -CH_2-$(CH_2)_8$-CH_3), 4.68 (t, $J=7.4$ Hz, 4H; -CH_2-$(CH_2)_9$-CH_3), 7.05 (d, $J=2.9$ Hz, 2H; pyrazolyl protons), 7.70 (d, $J=2.9$ Hz, 2H; pyrazolyl protons), 7.86 (d, $J=8.0$ Hz, 2H; pyridyl protons), 8.22 ppm (t, $J=$ 8.0 Hz, 1H; pyridyl proton); MS (FAB$^+$): m/z: 751 $[M-PF_6]^+$; elemental analysis calcd (%) for $C_{33}H_{53}N_5ClPF_6Pt$: C 44.27, H 5.93, N 7.83; found: C 44.65, H 6.37, N 7.87.

[Pt(N5C12)Cl]PF_6 (6): The procedure was similar to that for **2** except that N5C12 (225 mg, 0.41 mmol) was used in place of N5C4. Subsequent recrystallization by vapor diffusion of diethyl ether into a solution of the product in dichloromethane gave **6** as a pale yellow solid. Yield: 136 mg, 40%. ^{1}H NMR (400 MHz, $CDCl_3$, 298 K, relative to Me_4Si): $\delta=0.87$ (t, $J=6.5$ Hz, 6H; -CH_3), 1.24–1.32 (m, 36H; -$(CH_2)_9$-CH_3), 1.89–1.92 (m, 4H; -CH_2-$(CH_2)_9$-CH_3), 4.65 (t, $J=7.2$ Hz, 4H; -CH_2-$(CH_2)_{10}$-CH_3), 7.02 (d, $J=2.9$ Hz, 2H; pyrazolyl protons), 7.72 (d, $J=2.9$ Hz, 2H; pyrazolyl protons), 7.83 (d, $J=8.0$ Hz, 2H; pyridyl protons), 8.18 ppm (t, $J=$ 8.0 Hz, 1H, pyridyl proton); MS (FAB$^+$): m/z: 779 $[M-PF_6]^+$; elemental analysis calcd (%) for $C_{35}H_{57}N_5ClPF_6Pt$: C 45.53, H 6.22, N 7.58; found: C 45.49, H 6.23, N 7.74.

[Pt(N5C14)Cl]PF_6 (7): The procedure was similar to that for **2** except that N5C14 (247 mg, 0.41 mmol) was used in place of N5C4. Subsequent recrystallization by vapor diffusion of diethyl ether into a solution of the product in dichloromethane gave **7** as a pale yellow solid. Yield: 145 mg, 40%. ^{1}H NMR (400 MHz, $CDCl_3$, 298 K, relative to Me_4Si): $\delta=0.87$ (t, $J=6.5$ Hz, 6H; -CH_3), 1.24–1.33 (m, 44H; -$(CH_2)_{11}$-CH_3), 1.89–1.93 (m, 4H; -CH_2-$(CH_2)_{11}$-CH_3), 4.67 (t, $J=7.4$ Hz , 4H; -CH_2-$(CH_2)_{12}$-CH_3), 7.04 (d, $J=2.9$ Hz, 2H; pyrazolyl protons), 7.71 (d, $J=2.9$ Hz, 2H; pyrazolyl protons), 7.85 (d, $J=8.0$ Hz, 2H; pyridyl protons), 8.28 ppm (t, $J=$ 8.0 Hz, 1H; pyridyl proton); MS (FAB$^+$): m/z: 835 $[M-PF_6]^+$; elemental analysis calcd (%) for $C_{39}H_{65}N_5ClPF_6Pt$: C 47.83, H 6.64, N 7.15; found: C 48.29, H 6.67, N 7.20.

[Pt(N5C16)Cl]PF_6 (8): The procedure was similar to that for **2** except that N5C16 (270 mg, 0.41 mmol) was used in place of N5C4. Subsequent recrystallization by vapor diffusion of diethyl ether into a solution of the product in dichloromethane gave **8** as a pale yellow solid. Yield: 115 mg, 30%. ^{1}H NMR (400 MHz, $CDCl_3$, 298 K, relative to Me_4Si): $\delta=0.87$ (t, $J=6.8$ Hz, 6H; -CH_3), 1.24–1.33 (m, 52H; -$(CH_2)_{13}$-CH_3), 1.89–1.92 (m, 4H; -CH_2-$(CH_2)_{13}$-CH_3), 4.68 (t, $J=7.4$ Hz, 4H; -CH_2-$(CH_2)_{14}$-CH_3), 7.00 (d, $J=2.9$ Hz, 2H; pyrazolyl protons), 7.71 (d, $J=2.9$ Hz, 2H; pyrazolyl protons), 7.85 (d, $J=8.0$ Hz, 2H; pyridyl protons), 8.21 ppm (t, $J=$ 8.0 Hz, 1H, pyridyl proton); MS (FAB$^+$): m/z: 891 $[M-PF_6]^+$; elemental analysis calcd (%) for $C_{43}H_{73}N_5ClPF_6Pt$: C 49.88, H 7.06, N 6.77; found: C 50.22, H 7.24, N 6.78.

[Pt(N5C18)Cl]PF_6 (9): The procedure was similar to that for **2** except that N5C18 (293 mg, 0.41 mmol) was used in place of N5C4. Subsequent recrystallization by vapor diffusion of diethyl ether into a solution of the

product in dichloromethane gave **9** as a pale yellow solid. Yield: 81 mg, 20%. ^{1}H NMR (400 MHz, [D$_6$]DMSO–CDCl$_3$ 1:2 v/v, 298 K, relative to Me$_4$Si): δ = 0.87 (t, J = 6.8 Hz, 6H; -CH_3,), 1.24–1.34 (m, 60H; -(CH_2)$_{15}$-CH$_3$), 1.89–1.93 (m, 4H; -CH_2-(CH$_2$)$_{15}$-CH$_3$), 4.76 (t, J = 7.4 Hz, 4H; -CH_2-(CH$_2$)$_{16}$-CH$_3$), 7.29 (d, J = 2.9 Hz, 2H; pyrazolyl protons), 8.10 (d, J = 8.0 Hz, 2H; pyrazolyl protons), 8.32 (d, J = 2.9 Hz, 2H; pyridyl protons), 8.21 ppm (t, J = 8.0 Hz, 1H, pyridyl proton); MS (FAB$^+$): m/z: 947 [M−PF$_6$]$^+$; elemental analysis calcd (%) for C$_{47}$H$_{81}$N$_5$ClPF$_6$Pt·3/4CH$_2$Cl$_2$: C 49.64, H 7.20, N 6.06; found: C 49.59, H 7.27, N 6.29.

[Pt(N5C1)(C≡C-C$_6$H$_5$)]PF$_6$ (10): Phenylacetylene (50 mg, 0.50 mmol), a catalytic amount of CuI (2 mg) and NEt$_3$ (0.5 mL) were added to a degassed solution of **1** (200 mg, 0.32 mmol) in DMF (5–8 mL). The resultant solution was stirred at RT for 12 h and diethyl ether (60 mL) was added. A greenish-yellow precipitate was obtained, which was filtered and redissolved in a minimum amount of MeOH, followed by a metathesis reaction with NH$_4$PF$_6$. Subsequent recrystallization by vapor diffusion of diethyl ether into a solution of the product in acetone gave **10** as greenish-yellow crystals. Yield: 150 mg, 69%. ^{1}H NMR (400 MHz, CD$_3$CN, 298 K, relative to Me$_4$Si): δ = 4.33 (s, 6H; -CH_3), 7.03 (d, J = 2.8 Hz, 2H; pyrazolyl protons), 7.33–7.46 (m, 3H; phenyl protons), 7.48 (m, 2H; phenyl protons), 7.83 (d, J = 8.0 Hz, 2H; pyridyl protons), 7.86 (d, J = 2.8 Hz, 2H; pyrazolyl protons), 8.20 ppm (t, J = 8.0 Hz, 1H; pyridyl proton); MS (FAB$^+$): m/z: 680 [M−PF$_6$]$^+$; elemental analysis calcd (%) for C$_{21}$H$_{18}$F$_6$N$_5$PPt: C 37.07, H 2.67, N 10.29; found: C 36.78, H 2.74, N 10.36.

[Pt(N5C1)(C≡C-C$_6$H$_4$-CF$_3$-*p*)]PF$_6$ (11): The procedure was similar to that for **10** except that 4-trifluorophenylacetylene (85 mg, 0.50 mmol) was used in place of phenylacetylene to give **11** as a pale yellow solid. Yield: 155 mg, 65%. ^{1}H NMR (400 MHz, CD$_3$CN, 298 K, relative to Me$_4$Si): δ = 4.36 (s, 6H; -CH_3), 7.09 (d, J = 2.8 Hz, 2H; pyrazolyl protons), 7.57 (d, J = 8.0 Hz, 2H; phenyl protons), 7.76 (d, J = 8.0 Hz, 2H; phenyl protons), 7.90–7.92 (m, 4H; pyridyl and pyrazolyl protons), 8.26 ppm (t, J = 8.0 Hz, 1H; pyridyl proton); MS (FAB$^+$): m/z: 603 [M−PF$_6$]$^+$; elemental analysis calcd (%) for C$_{22}$H$_{17}$F$_9$N$_5$PPt: C 35.30, H 2.29, N 9.36; found: C 35.11, H 2.32, N 9.37.

[Pt(N5C1)(C≡C-C$_6$H$_4$-N(C$_6$H$_5$)$_2$-*p*)]PF$_6$ (12): The procedure was similar to that for **10** except that 4-ethynylphenyldiphenylamine (135 mg, 0.50 mmol) was used in place of phenylacetylene to give **12** as a pale yellow solid. Yield: 176 mg, 65%. ^{1}H NMR (400 MHz, CD$_3$CN, 298 K, relative to Me$_4$Si): δ = 4.40 (s, 6H; -CH_3), 7.06 (d, J = 8.6 Hz, 2H; phenyl protons), 7.09 (d, J = 2.8 Hz, 2H; pyrazolyl protons), 7.21 (d, J = 8.8 Hz, 6H; phenyl protons), 7.30 (d, J = 8.6 Hz, 2H; phenyl protons), 7.45 (d, J = 8.8 Hz, 4H; phenyl protons), 7.89–7.91 (m, 4H; pyridyl and pyrazolyl protons), 8.25 ppm (t, J = 8.0 Hz, 1H; pyridyl proton); IR (KBr): $\tilde{\nu}$ = 2124 (w) ν(C≡C), 753 cm^{-1} (s) ν(P–F); MS (FAB$^+$): m/z: 702 [M−PF$_6$]$^+$; elemental analysis calcd (%) for C$_{33}$H$_{27}$F$_6$N$_6$PPt: C 46.76, H 3.21, N 9.91; found: C 46.38, H 3.24, N 9.96.

[Pt(N5C14)(C≡C-C$_6$H$_5$)]PF$_6$ (13): Phenylacetylene (25 mg, 0.24 mmol), a catalytic amount of CuI (2 mg) and triethylamine (0.5 mL) were added to a degassed solution of **7** (150 mg, 0.15 mmol) in dichloromethane (50 mL). The resultant solution was stirred at room temperature under N$_2$ overnight. After evaporation of the solvent, the residue was purified by column chromatography on silica gel using dichloromethane-acetone (12:1 v/v) as eluent to give a yellow solid. Recrystallization by vapor diffusion of diethyl ether into a solution of the product in dichloromethane gave **13** as a yellow solid. Yield: 65 mg, 45%. ^{1}H NMR (500 MHz, CD$_3$CN, 298 K, relative to Me$_4$Si): δ = 0.90 (t, J = 6.9 Hz, 6H; -CH_3), 1.14–1.31 (m, 48H; -(CH_2)$_{12}$-CH$_3$), 4.84 (t, J = 7.4 Hz, 4H; -CH_2-(CH$_2$)$_{12}$-CH$_3$), 7.07 (d, J = 2.6 Hz, 2H; pyrazolyl protons), 7.25–7.27 (m, H; phenyl protons), 7.33–7.38 (m, 4H; phenyl protons), 7.87–7.89 (m, 4H, pyridyl and pyrazolyl protons), 8.22 ppm (t, J = 8.0 Hz, 1H; pyridyl proton); IR (KBr): $\tilde{\nu}$ = 2125 (w) ν(C≡C), 754 (s) ν(P-F); MS (FAB$^+$): m/z: 899 [M−PF$_6$]$^+$; elemental analysis calcd (%) for C$_{47}$H$_{70}$N$_5$PF$_6$Pt: C 54.01, H 6.75, N 6.70; found: C 53.66, H 6.65, N 6.68.

Physical measurements and instrumentation: ^{1}H NMR spectra were recorded on a Bruker DPX 400 FT-NMR spectrometer (400 MHz) or a Bruker Avance 500 instrument (500 MHz) at 298 K with chemical shifts reported relative to tetramethylsilane, Me$_4$Si. All positive ion FABMS and EIMS were recorded on a Finnigan MAT95 mass spectrometer. Elemental analyses were performed on a Flash EA1112 from ThermoQuest Italia SPA at the Changchun Institute of Applied Chemistry or a Carlo Erba 1106 elemental analyzer at the Institute of Chemistry, Chinese Academy of Sciences. The UV/Vis absorption spectra were obtained by using a Hewlett–Packard 8452 A diode array spectrophotometer or a Shimadzu 3100 PC spectrophotometer. Steady-state excitation and emission spectra at RT were recorded on a Spex Fluorolog-2 Model F111 fluorescence spectrofluorometer equipped with a Hamamatsu R-928 photomultiplier tube. All solutions for photophysical studies were prepared under high vacuum in a 10 cm^3 round-bottomed flask equipped with a sidearm 1 cm fluorescence cuvette and sealed from the atmosphere by a Rotaflo HP6/6 quick-release Teflon stopper. Solutions were rigorously degassed on a high-vacuum line in a two-compartment cell with no less than four successive freeze-pump-thaw cycles. Solid-state photophysical measurements were carried out with the solid sample loaded in a quartz tube inside a quartz-walled Dewar flask. Liquid nitrogen was placed into the Dewar flask for low temperature (77 K) photophysical measurements. Excited-state lifetimes of solution samples were measured by using a conventional laser system. The excitation source used was the 355 nm output (third harmonic, 8 ns) of a Spectra-Physics Quanta-Ray Q-switched GCR-150 pulsed Nd:YAG laser (10 Hz). Cyclic voltammetric measurements were performed by using a CH Instruments, Inc. model CHI 600A electrochemical analyzer. The electrolytic cell used was a conventional two-compartment cell. Electrochemical measurements were performed in acetonitrile with 0.1 M nBu$_4$NPF$_6$ (TBAH) as supporting electrolyte at RT. The reference electrode was a Ag/AgNO$_3$ (0.1 M in acetonitrile) electrode, and the working electrode was a glassy carbon electrode (CH Instruments, Inc.) with a platinum wire as the counter electrode. The working electrode surface was first polished with 1 μm alumina slurry (Linde), followed by 0.3 μm alumina slurry, on a microcloth (Buehler Co.). Treatment of the electrode surfaces was as reported previously.[21a] The ferrocenium/ferrocene couple (FeCp$_2^{+/0}$) was used as the internal reference.[21b] All solutions for electrochemical studies were deaerated with prepurified argon gas just before measurements. XRD was performed on a Rigaku X-ray diffractometer (D/max r A, by using Cu$_{K\alpha}$ radiation at a wavelength of 1.542 Å), and the data were collected from 0.7 to 10°. XPS was performed on a VG ESCA LAB MK-II spectrometer at a pressure of 10^{-7} Pa. Al$_{K\alpha}$ (1486.5 eV) was used as the excitation source, and the resolution of scanning was 0.05 eV. The binding energy of the sample was corrected, on the basis of the adventitious carbon (C 1s), to 284.6 eV. FTIR spectral measurements were performed on a Bruker VERTEX 80 V FTIR spectrometer equipped with a mercury–cadmium–telluride (MCT) detector (256 scans), recorded at a resolution of 4 cm^{-1}. Polarized IR measurements were made at incident angles of 0 and 60°, respectively, by using a polarizer attachment.

Preparation of LB film: A Nima 622D trough equipped with a Wilhelmy balance as surface pressure sensor was employed for surface pressure–molecular area isotherm measurements and the deposition of LB films. Solutions (1 mg mL^{-1}) of **7** and **13** in chloroform were prepared. After spreading the sample solution onto the water subphase, the monolayer was kept at the air–water interface for 20 min to allow the complete evaporation of the solvent and was then compressed with a constant barrier rate of 20 cm^2 min^{-1}. The temperature of the subphase was kept at (20 ± 0.5) °C. All the isotherms were repeated at least 3 times. The Langmuir monolayer was then allowed to stabilize for 15 min at the target pressure, and the condensed monolayer was finally transferred by the vertical dipping method onto a quartz substrate for UV/Vis absorption, XRD, and XPS measurements, and onto a CaF$_2$ substrate for IR and polarized IR measurements. In all cases, the dipping rate was set at 6 mm min^{-1}. The transfer ratios are reproducible and approach unity (0.9–1) in the repeated deposition cycles.

Crystal structure determination: Single crystals of **1**, **2**, and **10** were obtained by vapor diffusion of diethyl ether into a solution of the compounds in methanol–acetonitrile (1:1 v/v), dichloromethane solution, and acetonitrile solution of the respective complexes. The X-ray diffraction data were collected either on a Rigaku R-AXIS RAPID IP diffractometer (**1** and **2**) at 28 °C or on a Bruker Smart CCD 1000 (**10**) at 20 °C, both using graphite monochromatized Mo$_{K\alpha}$ radiation (λ = 0.71073 Å).

Table 5. Crystallographic and structural refinement data for complexes **1**, **2**, and **10**.

Complex	**1**	**2**	**10**·CH_3CN
empirical formula	$C_{14}H_{13}ClF_3N_5O_3SPt$	$C_{19}H_{23}ClN_5F_6PPt$	$C_{23}H_{21}F_6N_6PPt$
F_w	618.89	698.94	721.52
T [K]	293(2)	293(2)	301(2)
λ [Å]	0.71073	0.71073	0.71073
crystal system	monoclinic	monoclinic	orthorhombic
space group	$P2_1/c$	$C2/m$	$Pbcn$
a [Å]	7.0633(14)	14.115(3)	22.510(5)
b [Å]	23.348(5)	24.192(5)	15.623(3)
c [Å]	22.754(5)	8.8063(18)	14.574(3)
α [°]	90	90	90
β [°]	97.05(3)	126.66(3)	90
γ [°]	90	90	90
V [Å^3]	3724.1(14)	2412.3(9)	5125.3(18)
Z	8	4	8
ρ_{calcd} [g cm^{-3}]	2.208	1.925	1.870
μ [mm^{-1}]	7.847	6.057	5.606
$F(000)$	2351	1352	2784
crystal size [mm^3]	0.26×0.11×0.11	0.17×0.14×0.13	0.50×0.10×0.05
index ranges	$-7\le h\le 9$	$-18\le h\le 18$	$-18\le h\le 27$
	$-29\le k\le 30$	$31\le k\le 31$	$-19\le k\le 19$
	$-29\le l\le 30$	$-11\le l\le 11$	$-17\le l\le 17$
no. of reflns collected	35294	12004	25379
no. of indep reflns	8470	2832	4858
GOF on F^2	1.028	1.183	1.014
final R indices [$I>2\sigma(I)$]	$R_1=0.0634$	$R_1=0.0231$	$R_1=0.0286$
	$wR=0.1187$	$wR=0.0721$	$wR=0.0629$
largest diff. peak and hole [eÅ^{-3}]	2.113 and −0.817	0.888 and −0.583	1.203 and −0.624

The images were interpreted and intensities integrated by use of the program DENZO.[22] The structure was solved by direct methods employing the SHELXS-97 program.[23] Full-matrix least-squares refinement on F^2 was used in the structure refinement by program SHELXL-97.[24] The positions of H atoms were calculated on the basis of the riding mode with thermal parameters equal to 1.2 times those of the associated C atoms and participated in the calculation of final R indices. In the final stage of least-squares refinement, all non-hydrogen atoms were refined anisotropically. Crystallographic and structural refinement data are given in Table 5. CCDC-763143 (**1**), 763144 (**2**), and 763145 (**10**) contain the supplementary crystallographic data for this paper. These data can be obtained free of charge from The Cambridge Crystallographic Data Centre via www.ccdc.cam.ac.uk/data_request/cif.

Acknowledgements

V.W.-W.Y. acknowledges support from The University of Hong Kong under the Distinguished Research Achievement Award Scheme and the URC Strategic Research Theme on Molecular Materials. This work has been supported by the University Grants Committee Areas of Excellence Scheme (AoE/P-03/08) and the National Natural Science Foundation of China and the Research Grants Council of Hong Kong Joint Research Scheme (NSFC-RGC project no.: N HKU 737/06).

[1] a) D. M. Roundhill, H. B. Gray, C. M. Che, *Acc. Chem. Res.* **1989**, *22*, 55; b) G. Magnus, *Pog. Ann.* **1928**, *14*, 239; c) C. L. Exstrom, J. R. Sowa, Jr., C. A. Daws, D. Janzen, K. R. Mann, G. A. Moore, F. F. Stewart, *Chem. Mater.* **1995**, *7*, 15; d) C. E. Buss, C. E. Anderson, M. K. Pomije, C. M. Lutz, D. Britton, K. R. Mann, *J. Am. Chem. Soc.* **1998**, *120*, 7783; e) C. E. Buss, K. R. Mann, *J. Am. Chem. Soc.* **2002**, *124*, 1031.

[2] a) R. S. Osborn, D. Rogers, *J. Chem. Soc. Dalton Trans.* **1974**, 1002; b) R. H. Herber, M. Croft, M. J. Coyer, B. Bilash, A. Sahiner, *Inorg. Chem.* **1994**, *33*, 2422; c) W. B. Connick, R. E. Marsh, W. P. Schaefer, H. B. Gray, *Inorg. Chem.* **1997**, *36*, 913.

[3] a) H. Kunkely, A. Vogler, *J. Am. Chem. Soc.* **1990**, *112*, 5625; b) V. M. Miskowski, V. H. Houlding, *Inorg. Chem.* **1989**, *28*, 1529; c) V. M. Miskowski, V. H. Houlding, *Inorg. Chem.* **1991**, *30*, 4446; d) C. W. Chan, L. K. Cheng, C. M. Che, *Coord. Chem. Rev.* **1994**, *132*, 87.

[4] a) H. K. Yip, L. K. Cheng, K. K. Cheung, C. M. Che, *J. Chem. Soc. Dalton Trans.* **1993**, 2933; b) J. A. Bailey, M. G. Hill, R. E. Marsh, V. M. Miskowski, W. P. Schaefer, H. B. Gray, *Inorg. Chem.* **1995**, *34*, 4591.

[5] a) V. W. W. Yam, R. P. L. Tang, K. M. C. Wong, K. K. Cheung, *Organometallics* **2001**, *20*, 4476; b) V. W. W. Yam, K. M. C. Wong, N. Zhu, *J. Am. Chem. Soc.* **2002**, *124*, 6506; c) V. W. W. Yam, K. H. Y. Chan, K. M. C. Wong, N. Zhu, *Chem. Eur. J.* **2005**, *11*, 4535; d) K. M. C. Wong, W. S. Tang, B. W. K. Chu, N. Zhu, V. W. W. Yam, *Organometallics* **2004**, *23*, 3459.

[6] a) C. Yu, K. M. C. Wong, K. H. Y. Chan, V. W. W. Yam, *Angew. Chem.* **2005**, *117*, 801; *Angew. Chem. Int. Ed.* **2005**, *44*, 791; b) C. Yu, K. H. Y. Chan, K. M. C. Wong, V. W. W. Yam, *Chem. Eur. J.* **2008**, *14*, 4577; c) C. Yu, K. H. Y. Chan, K. M. C. Wong, V. W. W. Yam, *Proc. Natl. Acad. Sci. USA* **2006**, *103*, 19657; d) V. W. W. Yam, K. H. Y. Chan, K. M. C. Wong, B. W. K. Chu, *Angew. Chem.* **2006**, *118*, 6315; *Angew. Chem. Int. Ed.* **2006**, *45*, 6169; e) A. Y. Y. Tam, K. M. C. Wong, G. Wang, V. W. W. Yam, *Chem. Commun.* **2007**, 2028; f) A. Y. Y. Tam, K. M. C. Wong, G. Wang, N. Zhu, V. W. W. Yam, *Langmuir* **2009**, *25*, 8685; g) K. H. Y. Chan, J. W. Y. Lam, K. M. C. Wong, B. Z. Tang, V. W. W. Yam, *Chem. Eur. J.* **2009**, *15*, 2328.

[7] a) A. Y. Y. Tam, K. M. C. Wong, V. W. W. Yam, *J. Am. Chem. Soc.* **2009**, *131*, 6253; b) A. Y. Y. Tam, K. M. C. Wong, V. W. W. Yam, *Chem. Eur. J.* **2009**, *15*, 4775.

[8] a) W. S. Tang, X. X. Lu, K. M. C. Wong, V. W. W. Yam, *J. Mater. Chem.* **2005**, *15*, 2714; b) K. M. C. Wong, W. S. Tang, X. X. Lu, N. Zhu, V. W. W. Yam, *Inorg. Chem.* **2005**, *44*, 1492; c) H. S. Lo, S. K. Yip, K. M. C. Wong, N. Zhu, V. W. W. Yam, *Organometallics* **2006**, *25*, 3537.

[9] a) K. W. Jennette, S. J. Lippard, G. A. Vassiliades, W. R. Bauer, *Proc. Natl. Acad. Sci. USA* **1974**, *71*, 3839; b) K. W. Jennette, J. T. Gill, J. A. Sadownick, S. J. Lippard, *J. Am. Chem. Soc.* **1976**, *98*, 6159; c) M. Cusumano, M. L. D. Pietro, A. Giannetto, *Inorg. Chem.* **1999**, *38*, 1754; d) K. Becker, C. Herold-Mende, J. J. Park, G. Lowe, R. H. Schirmer, *J. Med. Chem.* **2001**, *44*, 2784; e) D. L. Ma, C. M. Che, *Chem. Eur. J.* **1999**, *5*, 6133; f) E. M. A. Ratilla, H. M. Brothers II, N. M. Kostic, *J. Am. Chem. Soc.* **1987**, *109*, 4592.

[10] a) K. Wang, M. A. Haga, H. Monjushiro, M. Akiba, Y. Sasaki, *Inorg. Chem.* **2000**, *39*, 4022; b) L. J. Grove, J. M. Rennekamp, H. Jude, W. B. Connick, *J. Am. Chem. Soc.* **2004**, *126*, 1594; c) E. J. Rivera, C. Figueroa, J. L. Colón, L. Grove, W. B. Connick, *Inorg. Chem.* **2007**, *46*, 8569; d) V. G. Vaidyanathan, B. U. Nair, *Eur. J. Inorg. Chem.* **2005**, 3756.

[11] a) S. C. Yu, S. Hou, W. K. Chan, *Marcomolecules* **1999**, *32*, 5251; b) M. A. Haga, H. G. Hong, Y. Shiozawa, Y. Kawata, H. Monjushiro, T. Fukuo, R. Arakawa, *Inorg. Chem.* **2000**, *39*, 4566.
[12] a) C. Piguet, G. Bernardinelli, A. F. Williams, *Inorg. Chem.* **1989**, *28*, 2920; b) C. Piguet, B. Bocquet, E. Müller, A. F. Williams, *Helv. Chim. Acta* **1989**, *72*, 323; c) S. R. Wittmann, C. Piguet, G. Bernardinelli, B. Bocquet, A. F. Williams, *J. Am. Chem. Soc.* **1992**, *114*, 4230.
[13] a) A. W. Addison, S. Burman, C. G. Wahlgren, *J. Chem. Soc. Dalton Trans.* **1987**, 2621; b) S. Obara, M. Itabashi, F. Okuda, S. Tamaki, Y. Tanabe, Y. Ishii, K. Nozaki, M. A. Haga, *Inorg. Chem.* **2006**, *45*, 8907–8921.
[14] a) M. A. Halcrow, *Coord. Chem. Rev.* **2005**, *249*, 2880; b) S. A. Willison, H. Jude, R. M. Antonelli, J. M. Rennekamp, N. A. Eckert, J. A. K. Bauer, W. B. Connick, *Inorg. Chem.* **2004**, *43*, 2548.
[15] P. Gamez, R. H. Steensma, W. L. Driessen, J. Reedijk, *Inorg. Chim. Acta* **2002**, *333*, 51.
[16] H. L. Casal, D. G. Cameron, H. H. Mantsch, *J. Phys. Chem.* **1985**, *89*, 5557.
[17] R. A. MacPhail, H. L. Strauss, R. G. Snyder, C. A. Elliger, *J. Phys. Chem.* **1984**, *88*, 334.
[18] H. Hagemann, R. G. Snyder, A. J. Peacock, L. Mandelkern, *Macromolecules* **1989**, *22*, 3600.
[19] J. J. Benítez, S. Kopta, D. F. Ogletree, M. Salmeron, *Langmuir* **2002**, *18*, 6096.
[20] K. Onitsuka, N. Ohara, F. Takei, S. Takahashi, *Dalton Trans.* **2006**, 3693.
[21] a) C. M. Che, K. Y. Wong, F. C. Anson, *J. Electroanal. Chem. Interfacial Electrochem.* **1987**, *226*, 211; b) N. G. Connelly, W. E. Geiger, *Chem. Rev.* **1996**, *96*, 877.
[22] Written with the cooperation of the program authors Z. Otwinowski, W. Minor: D. Gewirth DENZO: "The HKL Manuals-A description of programs DENZO, XDISPLAYF, and SCALEPACK", Yale University, New Haven, **1995**.
[23] SHELXS97, Programs for Crystal Structure Analysis, release 97-2, G. M. Sheldrick, University of Göttingen (Germany), **1997**.
[24] SHELXL97, Programs for Crystal Structure Analysis, release 97-2, G. M. Sheldrick, University of Göttingen, Göttingen (Germany), **1997**.

Received: January 26, 2010
Published online: May 21, 2010

